



Fast 5-minute shoulder MRI protocol with accelerated TSE-sequences and deep learning image reconstruction for the assessment of shoulder pain at 1.5 and 3 Tesla

Judith Herrmann^a, You-Shan Feng^b, Sebastian Gassenmaier^a, Jan-Peter Grunz^c, Gregor Koerzdoerfer^d, Andreas Lingg^a, Haidara Almansour^a, Dominik Nickel^d, Ahmed E. Othman^{a,e}, Saif Afat^{a,*}

^a Department of Diagnostic and Interventional Radiology, University Hospital Tuebingen, Eberhard Karls University, Tuebingen, Germany

^b Institute for Clinical Epidemiology and Applied Biometrics, University Hospital Tuebingen, Eberhard Karls University, Tuebingen, Germany

^c Department of Diagnostic and Interventional Radiology, University Hospital Würzburg, Würzburg, Germany

^d MR Application Predevelopment, Siemens Healthcare GmbH, Erlangen, Germany

^e Department of Neuroradiology, University Medical Center Mainz, Mainz, Germany

HIGHLIGHTS

- MRI has become the most commonly used imaging modality for patients with shoulder pain.
- Deep learning TSE reduces the scan time for the shoulder to 5 minutes.
- Deep learning TSE provides significant improvement of noise and image quality.
- Diagnostic performance of Deep Learning and standard TSE is interchangeable.
- This immense reduction in scan time increases patient throughput and patient comfort.

ARTICLE INFO

Keywords:

Acceleration
Magnetic resonance imaging
Deep learning reconstruction
Image processing
Diagnostic imaging

ABSTRACT

Purpose: The objective of this study was to implement a 5-minute MRI protocol for the shoulder in routine clinical practice consisting of accelerated 2D turbo spin echo (TSE) sequences with deep learning (DL) reconstruction at 1.5 and 3 Tesla, and to compare the image quality and diagnostic performance to that of a standard 2D TSE protocol.

Methods: Patients undergoing shoulder MRI between October 2020 and June 2021 were prospectively enrolled. Each patient underwent two MRI examinations: first a standard, fully sampled TSE (TSE_S) protocol reconstructed with a standard reconstruction followed by a second fast, prospectively undersampled TSE protocol with a conventional parallel imaging undersampling pattern reconstructed with a DL reconstruction (TSE_{DL}). Image quality and visualization of anatomic structures as well as diagnostic performance with respect to shoulder lesions were assessed using a 5-point Likert-scale (5 = best). Interchangeability analysis, Wilcoxon signed-rank test and kappa statistics were performed to compare the two protocols.

Results: A total of 30 participants was included (mean age 50±15 years; 15 men). Overall image quality was evaluated to be superior in TSE_{DL} versus TSE_S (p<0.001). Noise and edge sharpness were evaluated to be significantly superior in TSE_{DL} versus TSE_S (noise: p<0.001, edge sharpness: p<0.05). No difference was found concerning qualitative diagnostic confidence, assessability of anatomical structures (p>0.05), and quantitative diagnostic performance for shoulder lesions when comparing the two sequences.

Abbreviations: CS, Compressed Sensing; DL, Deep Learning; FA, Flip Angle; IQ, Image Quality; IQR, Interquartile Range; MRI, Magnetic Resonance Imaging; SNR, Signal-to-Noise Ratio; S, Standard; TA, Time of Acquisition; PD, Proton Density; T1w, T1-weighted; TSE, Turbo Spin Echo; PAT, Parallel Acquisition Technique; PI, Parallel Imaging.

* Correspondence to: Department of Diagnostic and Interventional Radiology, Tübingen University Hospital, Hoppe-Seyler-Str 3, Tübingen 72076, Germany

E-mail address: saif.afat@med.uni-tuebingen.de (S. Afat).

<https://doi.org/10.1016/j.ejro.2024.100557>

Received 5 September 2023; Received in revised form 13 February 2024; Accepted 18 February 2024

2352-0477/© 2024 The Author(s). Published by Elsevier Ltd. This is an open access article under the CC BY-NC license (<http://creativecommons.org/licenses/by-nc/4.0/>).

Conclusions: A fast 5-minute TSE_{DL} MRI protocol of the shoulder is feasible in routine clinical practice at 1.5 and 3 T, with interchangeable results concerning the diagnostic performance, allowing a reduction in scan time of more than 50% compared to the standard TSE_S protocol.

1. Introduction

Magnetic resonance imaging (MRI) of the shoulder has become the most commonly used imaging modality in patients with shoulder pain due to its ability to enable comprehensive noninvasive diagnosis of pathologies such as rotator cuff or biceps tendon tears, and glenoid labral abnormalities [1,2]. Standard MRI protocols for shoulder imaging consist of two-dimensional (2D) turbo spin-echo (TSE) sequences in three planes. A disadvantage of these comprehensive protocols is the long acquisition time of approximately 10–20 minutes. Methods to accelerate shoulder MRI acquisition primarily involve parallel imaging (PI), compressed sensing (CS), or three-dimensional (3D) MR sequences at high-resolution [3–7]. However, a major disadvantage of PI is the substantially lower signal-to-noise ratio (SNR) when accelerating sequences and, regarding 3D-sequences, the suboptimal tissue contrast [6].

Recently, novel MRI reconstruction techniques based on deep learning (DL) have been introduced and have revolutionized the trade-off between shortening acquisition time and maintaining image quality. The efficiency of DL acceleration for TSE-sequences has previously been evaluated for MRI protocols in musculoskeletal imaging of different joints, including protocols for shoulder imaging [8–14]. However, studies on the clinical implementation at 1.5 and 3 T and particularly on diagnostic performance in clinical practice for shoulder MRI are still scarce.

We hypothesize that a DL-reconstruction for TSE imaging of the shoulder is feasible in routine clinical practice and may allow for a significant reduction of examination time with comparable image quality and interchangeable diagnostic performance compared with standard imaging.

Therefore, the aim of this study was to implement a fast 5-minute shoulder MRI protocol consisting of accelerated 2D TSE sequences with DL-reconstruction at 1.5 and 3 T in daily clinical practice and to compare the image quality and diagnostic performance in terms of detection of common shoulder pathologies to that of a standard 2D TSE protocol.

2. Materials and methods

2.1. Study design

This single-center prospective study was approved by the institutional review board (clinical trial registry number: DRKS00023278) and written informed consent was obtained from all participants. All study procedures were in accordance with the Declaration of Helsinki and its subsequent amendments. Patients undergoing native MRI of the shoulder were consecutively enrolled in the study between October 2020 and June 2021. Inclusion criteria were clinically indicated shoulder MRI on appropriate scanners with the DL-reconstruction algorithm installed. Exclusion criteria were age under 18 years, application of contrast agents, nonconditional implants, and severe claustrophobia. The final sample included 30 participants (see Fig. 1 and Table 1).

2.2. MRI protocol

All MRI examinations were performed in routine clinical practice using 1.5 and 3 T MRI scanners (MAGNETOM Avanto^{fit}, MAGNETOM Aera, MAGNETOM Skyra, MAGNETOM Prisma^{fit}, and MAGNETOM Vida, Siemens Healthcare, Erlangen, Germany). Patients were examined

Table 1

Patients' characteristic.

Patients (male/female), n	30 (15/15)
Scanner (1.5 T/3 T), n	15/15
Age, mean ± SD (range), y	total: 50 ± 15 (22–76) male: 55 ± 15 (33–76) female: 45 ± 15 (22–65)
Shoulder (right/left), n	15/15
Indication of MRI, n	Impingement syndrome/calcific tendinitis, 11 Rotator cuff tendinopathy/tear, 9 Acute trauma, 4 Instability or dislocation, 3 Pain not otherwise specified, 3

n indicates number; T, Tesla; SD, standard deviation; y, years.

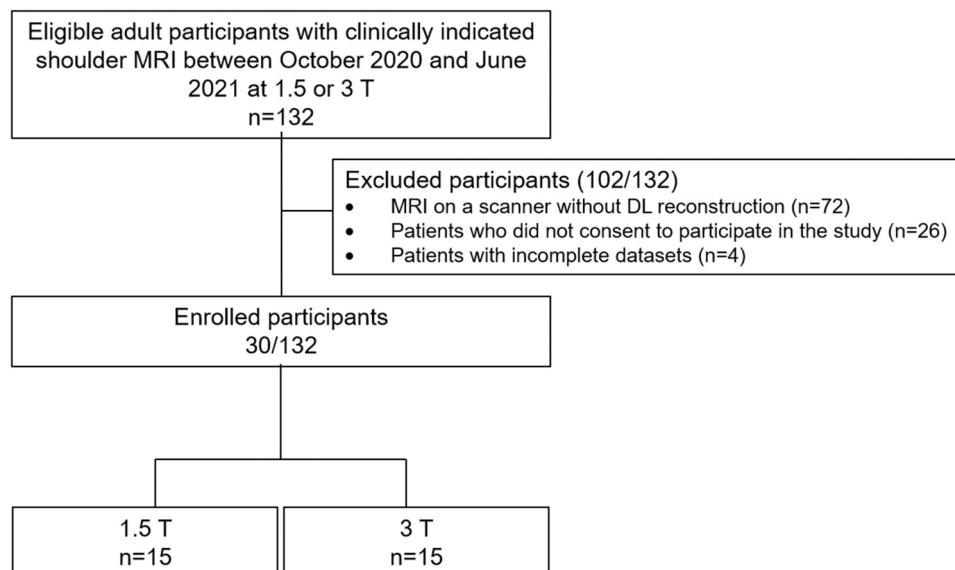


Fig. 1. Flow diagram of study inclusion and exclusion. DL = deep learning; T = Tesla.

in supine position with the arms in anatomical position using a 16-channel shoulder coil. All participants were examined with the institution's standard protocol (TSE_S) and the accelerated protocol with DL-reconstruction (TSE_{DL}). The TSE_S consisted of the following sequences: proton density (PD)-weighted TSE with fat saturation (FS) in three planes (axial, coronal, sagittal) as well as one coronal T1-weighted (T1w) TSE. Immediately after TSE_S, the same sequence protocol was acquired with undersampled TSE sequences and reconstructed on the scanner using the research DL-reconstruction (TSE_{DL}). The detailed MRI acquisition parameters are listed in Table 2. Siemens Healthineers, Erlangen, Germany provided the research DL-reconstruction. Full control of patient data was with the authors.

2.3. Deep learning-reconstruction technique for TSE

The undersampling pattern and the DL-reconstruction used for the fast 5-minute TSE_{DL} protocol in this study have been introduced in previous studies for TSE sequences [8, 11, 13, 15–18]. The *k*-space data are prospectively undersampled according to established patterns as known from parallel imaging [19, 20] and reconstructed using a DL-based image reconstruction with a fixed iterative reconstruction scheme or variational network [19, 21].

The reconstruction was trained on previous volunteer acquisitions using conventional TSE protocols. Approximately 10,000 slices were acquired on volunteers using different clinical 1.5 T and 3 T scanners (MAGNETOM scanners, Siemens Healthcare, Erlangen, Germany).

For use in the clinical setting, the trained network was converted to a proprietary C++ inference framework and integrated into the reconstruction pipeline of the scanners.

2.4. Image analysis

The thirty pairs of corresponding TSE_S and TSE_{DL} datasets were separated, anonymized, and randomized. Sixty individual studies were obtained. Each of these studies was independently assessed by two radiologists with 5 and 2 years of experience in musculoskeletal MRI interpretation. Readers were blinded to reconstruction type, clinical and

radiological report, and each other's assessment. Before evaluation, both readers completed a joint training session with ten complete examinations that were not included in this study. Image quality parameters were evaluated using the following criteria on a five-point Likert scale (5, excellent; 1, non-diagnostic): Overall image quality, artifacts, banding artifacts, edge sharpness, noise, and diagnostic confidence as well as image impression. Delineation of anatomic structures of the shoulder included rotator cuff tendons, long biceps tendon, glenoid labrum, glenohumeral joint, acromioclavicular joint, as well as lesser and greater tuberosity. The extent of delineation was rated using an ordinal five-point Likert scale (5, excellent delineation; 1, no delineation). Diagnostic performance was assessed by evaluating abnormalities of the rotator cuff tendons (supraspinatus, infraspinatus, subscapularis), long biceps tendon, and glenoid labrum for the presence of lesions using a three-point scale (0, normal; 1, degeneration; 2, tear). The acromioclavicular joint, the glenohumeral joint as well as the lesser and greater tuberosity were evaluated for the presence of lesions using a two-point scale (0, normal; 1, edema and/or subchondral cyst). Joint fluid and bone marrow edema were evaluated to be present or absent (0, absent; 1, present).

Image analysis was performed on a PACS workstation (GE Healthcare Centricity PACS RA1000, Milwaukee, WI, USA). Interpretation of the examinations for each subject was separated by a period of 6 weeks, and the readers were blinded to the other readers' evaluations to limit the potential for recall bias.

2.5. Statistical evaluation

Statistical evaluation was performed using SPSS Statistics Version 26 (IMB, Armonk, NY; USA), Stata Version 16 (StataCorp, Texas, USA), and R (v4.0.3, R Core Team, Vienna, Austria). Whereas parametric variables are displayed using mean ± standard deviation (SD), non-parametric variables are displayed using mean, median and interquartile range (IQR) in parentheses. The Wilcoxon signed-rank test was used for paired data of ordinal structure and non-normally-distributed parametric variables. The significance level was set at 0.05.

Kappa statistic is commonly used to assess interreader reliability

Table 2
Acquisition parameters.

Parameters									
Acquisition parameters of TSE _S and TSE _{DL} at 1.5 T									
	PD TSE _S FS	PD TSE _{DL} FS	PD TSE _S FS	PD TSE _{DL} FS	T1 TSE _S	T1 TSE _{DL}	PD TSE _S FS	PD TSE _{DL} FS	
Orientation	axial	axial	coronal	coronal	coronal	coronal	sagittal	sagittal	
TA, min:s	2:56	1:05	2:53	1:02	1:44	1:11	2:53	1:02	
TE/TR, ms	42/3800	51/3550	42/3290	42/3160	9.2/562	9.2/549	42/3290	42/3000	
FOV, mm ²	180	180	180	180	180	180	180	180	
Voxel size, mm ³	0.6×0.6×3.0	0.6×0.6×3.0	0.6×0.6×3.0	0.6×0.6×3.0	0.3×0.3×3.0	0.6×0.6×3.0	0.6×0.6×3.0	0.6×0.6×3.0	
FA, degree	150	150	150	150	150	150	150	150	
Averages	2	1	2	1	1	1	2	1	
PAT	2	3	2	3	2	3	2	3	
Turbo factor	9	9	9	10	3	3	9	9	
Echo spacing, ms	8.46	8.46	8.46	8.46	9.22	9.22	8.46	8.46	
Bandwidth, Hz/Px	191	191	191	191	211	211	191	191	
Acquisition parameters of TSE _S and TSE _{DL} at 3 T									
	PD _S TSE FS	PD TSE _{DL} FS	PD TSE _S FS	PD TSE _{DL} FS	T1 TSE _S	T1 TSE _{DL}	PD TSE _S FS	PD TSE _{DL} FS	
Orientation	axial	axial	coronal	coronal	coronal	coronal	sagittal	sagittal	
TA, min:s	3:02	0:56	2:56	1:38	2:09	1:10	2:50	1:32	
TE/TR, ms	40/3000	39/3400	38/3000	37/3000	11/523	11/531	51/3000	49/3000	
FOV, mm ²	200	200	200	200	160	160	160	160	
Voxel size, mm ³	0.5×0.5×3.0	0.5×0.5×3.0	0.4×0.4×3.0	0.4×0.4×3.0	0.4×0.4×3.0	0.4×0.4×3.0	0.4×0.4×3.0	0.4×0.4×3.0	
FA, degree	150	150	150	150	150	150	150	150	
Averages	1	1	1	1	1	1	1	0	
PAT	2	4	2	4	2	4	2	4	
Turbo factor	9	9	11	11	4	4	11	12	
Echo spacing, ms	9.98	7.75	12.6	12.4	11	11.1	12.6	12.1	
Bandwidth, Hz/Px	250	250	150	150	250	250	150	150	

TSE indicates turbo spin echo; T, Tesla; PD, proton density; DL, deep learning; FS, fat saturation; TA, acquisition time; FOV, field of view; TE/TR, echo time/repetition time; FOV, field of view; FA, flip angle; PAT, Parallel Acquisition Technique; Hz: Hertz; Px: Pixel.

because it accounts for chance agreements [22]. We used the weighted Kappa-statistic to test the agreement between TSE_S and TSE_{DL}, and both readers. We used the commonly accepted rules of thumb to interpret agreement as minimal to non-agreement if Kappa is smaller than 0.4, weak if Kappa is 0.4–0.59, moderate if Kappa is 0.6–0.79, and strong if Kappa > 0.8 [22].

2.6. Interchangeability analysis

In addition to agreement, we assessed interchangeability between the TSE_S and TSE_{DL} [7, 23–25]. First the interreader agreement when both readers used the TSE_{DL} (intra-protocol interreader agreement rate) was compared with the agreement when one reader used the TSE_{DL}, and the other used the TSE_S (interprotocol interreader agreement rate). The interprotocol (TSE_S vs. TSE_{DL}) interreader agreement rate was subtracted from the intraprotocol (TSE_S vs. TSE_S) interreader agreement rate, resulting in the individual equivalence index. A 95% confidence interval (95% CI) was calculated using bootstrapping methods with 10,000 repetitions, i.e., by repeating the calculation of the equivalence index 10,000 times based on a set of patients randomly sampled with replacement. The interreader agreement index and 95% CI were calculated for each individual score as well as for groupings. A smaller than 5% difference in rate of agreement was considered acceptable.

Table 3

Image quality, lesion detectability, and interreader agreement using Cohen’s Kappa for TSE_S/TSE_{DL}.

	Reader 1			Reader 2			Intraprotocol interreader agreement			
	TSE _S Mean, Median (IQR)	TSE _{DL} Mean, Median (IQR)	p-value	TSE _S Mean, Median (IQR)	TSE _{DL} Mean, Median (IQR)	p-value	TSE _S		TSE _{DL}	
							Cohens κ	95% CI	Cohens κ	95% CI
Overall image quality										
Image quality	4.27, 4 (4–5)	4.80, 5 (5–5)	<0.001	4.37, 4 (4–5)	4.83, 5 (5–5)	<0.001	0.834	[0.68;0.98]	0.89	[0.72;1.00]
Artifacts	4.50, 5 (4–5)	4.67, 5 (4–5)	0.10	4.57, 5 (4–5)	4.70, 5 (4–5)	0.16	0.789	[0.61;0.95]	0.93	[0.81;1.00]
Banding artifacts	4.93, 5 (5–5)	4.60, 5 (4–5)	0.004	4.90, 5 (5–5)	4.63, 5 (4–5)	0.02	0.783	[0.37;1.00]	0.82	[0.63;1.00]
Edge sharpness	4.47, 4 (4–5)	4.87, 5 (5–5)	<0.001	4.57, 5 (4–5)	4.80, 5 (5–5)	0.02	0.802	[0.59;0.96]	0.76	[0.45;1.00]
Noise	4.37, 4 (4–5)	4.90, 5 (5–5)	<0.001	4.40, 4 (4–5)	4.83, 5 (5–5)	<0.001	0.935	[0.82;1.00]	0.71	[0.35;1.00]
Diagnostic confidence	4.77, 5 (4.75–5)	4.87, 5 (5–5)	0.08	4.80, 5 (5–5)	4.90, 5 (5–5)	0.18	0.706	[0.40;1.00]	0.84	[0.53;1.00]
Image impression	4.83, 5 (5–5)	4.73, 5 (4–5)	0.08	4.80, 5 (5–5)	4.77, 5 (4.75–5)	0.56	0.667	[0.32;1.00]	0.73	[0.45;1.00]
Delineation of anatomic structures										
Rotator cuff tendons	4.80, 5 (5–5)	4.77, 5 (4.75–5)	0.32	4.73, 5 (4–5)	4.77, 5 (4.75–5)	0.32	0.815	[0.57;1.00]	0.81	[0.57;1.00]
Long biceps tendon	4.77, 5 (5–5)	4.83, 5 (5–5)	0.32	4.73, 5 (4.75–5)	4.77, 5 (4.75–5)	0.66	0.918	[0.76;1.00]	0.79	[0.52;1.00]
Glenoid labrum	4.70, 5 (4–5)	4.80, 5 (5–5)	0.08	4.60, 5 (4–5)	4.67, 5 (4–5)	0.16	0.783	[0.56;1.00]	0.67	[0.38;1.00]
Acromioclavicular joint	4.83, 5 (5–5)	4.80, 5 (5–5)	0.32	4.83, 5 (5–5)	4.80, 5 (5–5)	0.66	0.760	[0.44;1.00]	0.67	[0.32;1.00]
Glenohumeral joint	4.83, 5 (5–5)	4.90, 5 (5–5)	0.16	4.73, 4 (5–5)	4.80, 5 (5–5)	0.16	0.710	[0.41;1.00]	0.62	[0.23;1.00]
Lesser tuberosity	4.83, 5 (5–5)	4.77, 5 (4.75–5)	0.41	4.73, 4 (5–5)	4.80, 5 (5–5)	0.41	0.710	[0.44;1.00]	0.71	[0.40;1.00]
Greater tuberosity	4.80, 5 (5–5)	4.83, 5 (5–5)	0.56	4.77, 4.75 (5–5)	4.80, 5 (5–5)	0.56	0.902	[0.71;1.00]	0.67	[0.32;1.00]

IQR indicates interquartile range; TSE, turbo spin echo; S, standard; DL, deep learning.

Image quality grading: 1 = non-diagnostic, 2 = low image quality, non-diagnostic; 3 = minor image quality impairment, diagnostic; 4 = good image quality, diagnostic; 5 = excellent image quality, diagnostic)

Cohen’s κ, interreader-agreement (0–0.20 = poor agreement, 0.21–0.40 = fair agreement, 0.41–0.60 = moderate agreement, 0.61–0.80 = substantial agreement, 0.81–1 = (almost) perfect agreement)

3. Results

3.1. Patients’ characteristics

Thirty patients with shoulder pain (15 men, 15 women; mean patient age: 50 ± 15 years, range: 22 – 76 years) were consecutively recruited. Scans were performed on patients’ symptomatic side (right: 15, left: 15), (see Table 1). An image example of the institution’s standard protocol with TSE_S and TSE_{DL} is displayed in Fig. 2.

The results of the more experienced reader 2 are described in the following. All results can be found in the tables of this manuscript.

3.2. Qualitative image analysis

Intraprotocol interreader agreement regarding image quality parameters resulted in a Cohen’s kappa of 0.788 for TSE_S and 0.813 for TSE_{DL}. Overall image quality was evaluated to be significantly superior in TSE_{DL} compared to TSE_S with a median of 5 (IQR 5 – 5) versus a median of 4 (IQR 4 – 5; p<0.001). Image noise levels were evaluated to be significantly superior in TSE_{DL} compared to TSE_S with a median of 5 (IQR 5 – 5) for TSE_{DL} versus a median of 4 (IQR 4 – 5; p<0.001) for TSE_S. Edge sharpness was evaluated to be significantly superior in TSE_{DL} compared to TSE_S with a median of 5 (IQR 5 – 5) for TSE_{DL} versus a median of 4 (IQR 4 – 5; p=0.02) for TSE_S. No significant difference was found concerning the overall extent of artifacts in TSE_{DL} and TSE_S with a median of 5 (IQR 4 – 5; p=0.16). The extent of banding artifacts was

rated higher in TSE_{DL} with a median of 5 (IQR 4–5) versus a median of 5 (IQR 5–5) in TSE_S ($p < 0.05$). Diagnostic confidence was evaluated to be comparable in TSE_{DL} compared to TSE_S with a median of 5 (5–5, $p = 0.18$). There was no significant difference regarding the image impression of both sequences with a median of 5 (5–5) for TSE_S and with a median of 5 (4.75–5) for TSE_{DL} ($p = 0.56$). Concerning the delineation of anatomical structures, no significant difference was found between the two sequences TSE_S and TSE_{DL} ($p = 0.16–0.66$). Table 3 shows image quality results of both readers.

3.3. Interchangeability analysis

While interreader agreement ranged from 83.33–96.67% for different structures, intrareader agreement between TSE_{DL} and TSE_S was nearly identical with 80.00–93.33% for almost all of the evaluated structures. The CIs for all evaluated parameters were within the critical limit [-5%, +5%], indicating that TSE_{DL} and TSE_S are interchangeable (Table 4).

Table 4 shows detailed interprotocol intrareader agreement and interchangeability results with corresponding confidence intervals. Figs. 2–5 show examples of TSE_S and TSE_{DL}.

3.4. Acquisition time reduction

The acquisition time (TA) of the fast TSE_{DL} protocol was 4:21 min versus 10:26 min of TSE_S protocol for 1.5 T and 5:16 min versus 10:56 min of TSE_S protocol for 3 T. Thus, TA for a native shoulder MRI protocol using TSE_{DL} was reduced by 58% for 1.5 T and by 52% for 3 T compared to the standard TSE_S protocol. These scan times were selected from the standard examination without adjusting the parameters for each individual.

4. Discussion

This study investigated the feasibility and compared the image quality and diagnostic performance of a fast 5-minute 2D TSE imaging with DL-reconstruction of the shoulder at 1.5 and 3 T and demonstrated that TSE_{DL} imaging of the shoulder was feasible in daily clinical routine, with acquisition time reduced by more than 50% and improved image quality compared to TSE_S.

In recent years, various imaging techniques have been developed and investigated to shorten the acquisition time of musculoskeletal MRI. A long acquisition time may compromise image quality due to motion artifacts caused by patient discomfort due to prolonged immobility. Mainly isotropic 3D sequences using gradient-echo or TSE techniques have been developed and implemented, which allow high-quality

multiplanar reformat images in thin continuous slices to provide a good delineation of anatomical structures. To further accelerate the 3D acquisition, Lee et al. investigated the application of compressed sensing (CS) to a 3D-TSE sequence for shoulder MRI [6]. CS is an established method for accelerating MRI acquisitions, including 2D sequences, and is based on redundancy of imaging data. The main disadvantages of CS images are their unnatural appearance and the long computation processing time [26]. Although Lee et al. found no relevant compromise in image quality comparing 3D-TSE with CS to standard 3D-TSE, no significant difference was found in terms of motions artifacts, and acquisition time was reduced only by about 30%. In our study, apart from no significant difference in terms of artifact extent, acquisition time was reduced by over 50% compared to standard imaging.

The potential of the DL-reconstruction in musculoskeletal MRI has previously been demonstrated in several studies [8, 9, 11, 13, 14, 18], including Hahn et al. who first showed the applicability of this technique in shoulder MRI, providing a 67% scan time reduction with comparable image quality, artifacts, and diagnostic performance in a cohort of 105 participants when using a PI undersampling pattern with an acceleration factor of 4 and the DL-reconstruction [10]. Obama et al. compared the DL-reconstruction in their study when using a CS and a PI undersampling pattern, including 30 participants and showed an improved image quality when using the DL-reconstruction, and a significantly shorter scan time, when combining the CS undersampling with the DL-reconstruction compared to the PI undersampling pattern with the DL-reconstruction [12]. However, in the aforementioned studies, the authors used exclusively MR scanners of 3 T and, beyond that, Obama et al. did not include the detectability of pathologies in the evaluation and assessed image quality solely.

In our study, we applied the DL-reconstruction in daily clinical routine at 1.5 and 3 T using an PI-based method with high undersampling factors was used to accelerate the image acquisition. In our study, image quality could be improved and no difference was found in the delineation of anatomical structures and the detection of various pathologies, which is in line with the aforementioned studies. Furthermore, in our study, no difference in the extent of artifacts was observed. Moreover, image quality was actually improved when DL-reconstruction was used. A major disadvantage of PI is the loss of SNR with the increase in acceleration factor. This is accompanied by banding artifacts, a disadvantage of DL-reconstructed images in our study. Banding artifacts are characteristic artifacts that appear in the form of a stripe pattern aligned exactly with the phase-encoding direction and are particularly strong in the low-SNR regions of DL-reconstructed images [27]. Although one reader noted a significantly higher extent of banding artifacts in the images of the TSE_{DL} protocol compared to TSE_S, overall image quality and general extent of artifacts as well as the diagnostic

Table 4
Interprotocol intrareader agreement and interchangeability results concerning shoulder lesions using Cohen’s Kappa for TSE_S/TSE_{DL}.

	Interprotocol intrareader agreement				Interchangeability results			
	R1		R2		R1 vs R2	TSE _S vs TSE _{DL}	Index	95% CI
	Cohens κ	95% CI	Cohens κ	95% CI				
Supraspinatus tendon	0.85	[0.73;0.97]	0.94	[0.86;1.02]	83.33%	80.00%	3.33%	[-15.00;21.65]
Infraspinatus tendon	0.83	[0.59;1.07]	0.92	[0.76;1.08]	93.33%	90.00%	-3.33%	[-14.32;0.81]
Subscapularis tendon	0.81	[0.54;1.09]	0.81	[0.54;1.09]	90.00%	90.00%	<0.01%	[-17.04;16.90]
Long biceps tendon	0.72	[0.46;0.99]	0.89	[0.73;1.05]	90.00%	90.00%	<0.01%	[-15.33;15.43]
Glenoid labrum	0.76	[0.45;1.07]	0.76	[0.45;1.07]	90.00%	88.33%	-1.67%	[-15.61;18.71]
Acromioclavicular joint	0.83	[0.61;1.05]	0.91	[0.74;1.08]	90.00%	88.33%	1.67%	[-15.01;18.04]
Glenohumeral joint	0.79	[0.52;1.06]	0.79	[0.52;1.06]	93.33%	91.67%	-1.67%	[-16.25;19.11]
Lesser tuberosity	0.63	[0.18;1.09]	0.63	[0.18;1.09]	96.67%	93.33%	3.33%	[-18.47;24.57]
Greater tuberosity	0.86	[0.67;1.05]	0.86	[0.67;1.05]	93.33%	88.33%	5.00%	[-13.07;23.12]
Joint fluid	0.87	[0.69;1.05]	0.87	[0.69;1.05]	90.00%	90.00%	<0.01%	[-15.33;15.43]
Bone marrow edema	0.92	[0.78;1.07]	0.92	[0.78;1.07]	93.33%	93.33%	<0.01%	[-15.27;15.45]

TSE indicates turbo spin echo; S, standard; DL, deep learning; CI, confidence interval.

Cohen’s κ, (0–0.20 = poor agreement, 0.21–0.40 = fair agreement, 0.41–0.60 = moderate agreement, 0.61–0.80 = substantial agreement, 0.81–1 = (almost) perfect agreement)

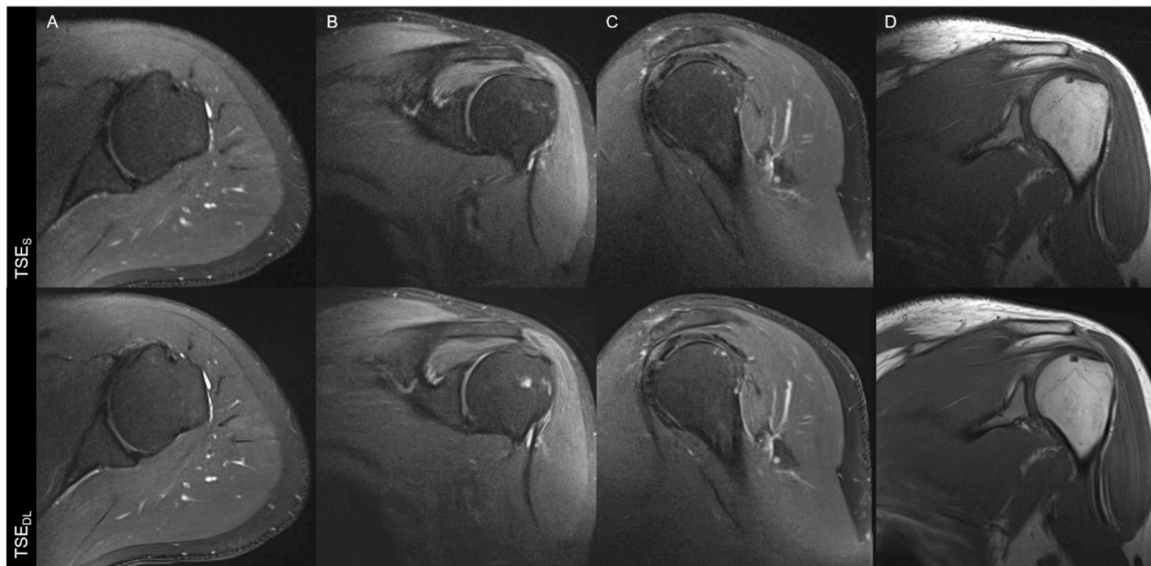


Fig. 2. Example of a standard (TSE_S , upper row) and accelerated, deep learning reconstructed (TSE_{DL} , lower row) shoulder MRI protocol with PD-weighted TSE sequences in axial (A), coronal (B), and sagittal oblique (C) orientation, as well as T1-weighted TSE in coronal orientation (D) of a 37-year-old patient with shoulder pain after trauma at 1.5 Tesla.

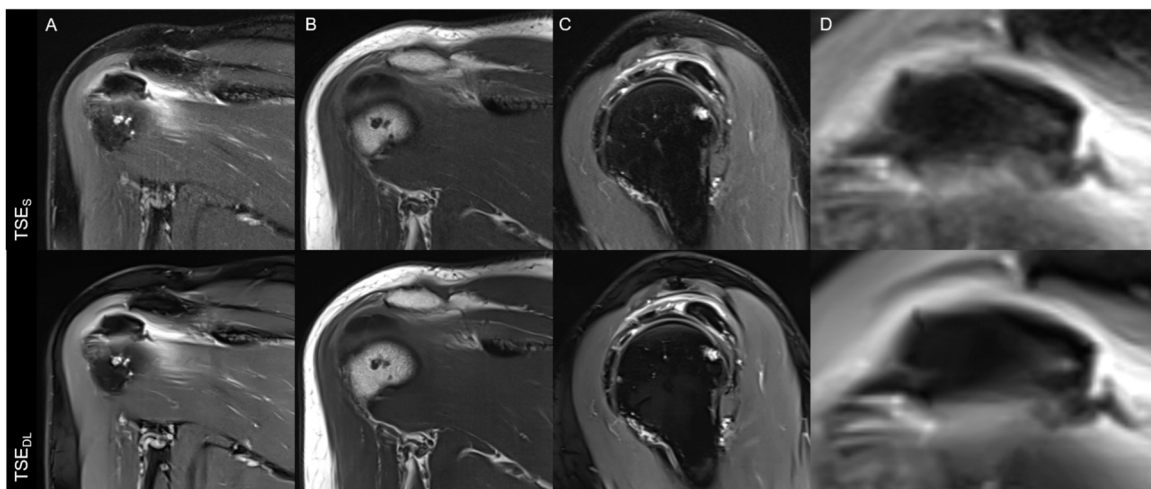


Fig. 3. Example of a standard (TSE_S , upper row) and accelerated, deep learning reconstructed (TSE_{DL} , lower row) shoulder MRI of the right shoulder at 3 Tesla of a 59-year-old female patient with pain and impingement symptoms. PD-weighted TSE sequences are displayed in axial (A), coronal (B), and sagittal oblique (C) orientation, as well as T1-weighted TSE in coronal orientation (D). In both, TSE_S and TSE_{DL} , a structure hypointense in PD- and T1-weighted TSE is seen in the cranial portion of the infraspinatus tendon measuring approximately 9×20 mm. Comparing TSE_S and TSE_{DL} noise is significantly reduced in TSE_{DL} and findings as the calcified structure can be very well delineated in both sequences, with the TSE_{DL} providing improved edge sharpness.

confidence of the images were not affected. Therefore, it can be assumed that the appearance of banding artifacts does not affect the image quality and the detection of pathological findings. Moreover, recent approaches have shown promising results in reducing such banding artifacts [27].

Despite the reduction in acquisition time and improved image quality, the question arises as to what clinical benefit can be derived from these results. MRI of the shoulder is an important tool for diagnosing the most common causes of shoulder pain, such as impingement syndrome or rotator cuff tears, and plays an important role in therapy planning [1, 2, 28, 29]. However, increasing demand for examinations does not automatically lead to an increase in supply because of limited availability of MRI scanners and examination times. To our knowledge, our study is the first to evaluate the implementation of DL-reconstruction on undersampled sequences for the shoulder in a prospective setting in daily clinical practice at both 1.5 and 3 T.

DL-reconstruction could be implemented in the clinical workflow, and during reconstruction, the MR-scanner could acquire subsequent sequences without interfering with the ongoing scanning workflow. In addition, the demonstrated approach of acquisition time reduction of more than 50% for multiplane, multicontrast imaging of the shoulder offers tremendous potential to increase scanner availability. Furthermore, reduced acquisition time proves to be an important advantage concerning patient comfort when examining patients who are sensitive to closed spaces, particularly among children.

Nonetheless, our study was not without limitations. First, although our 5-minute TSE_{DL} -protocol was comparable with TSE_S for all structures evaluated, the small sample size and the low prevalence of abnormalities, such as rotator cuff tears may limit the generalizability of the findings. Second, solely DL-reconstructions of T1- and PD-weighted 2D TSE imaging were examined in this study. However, due to the time-consuming acquisition process of PD-weighted sequences, these

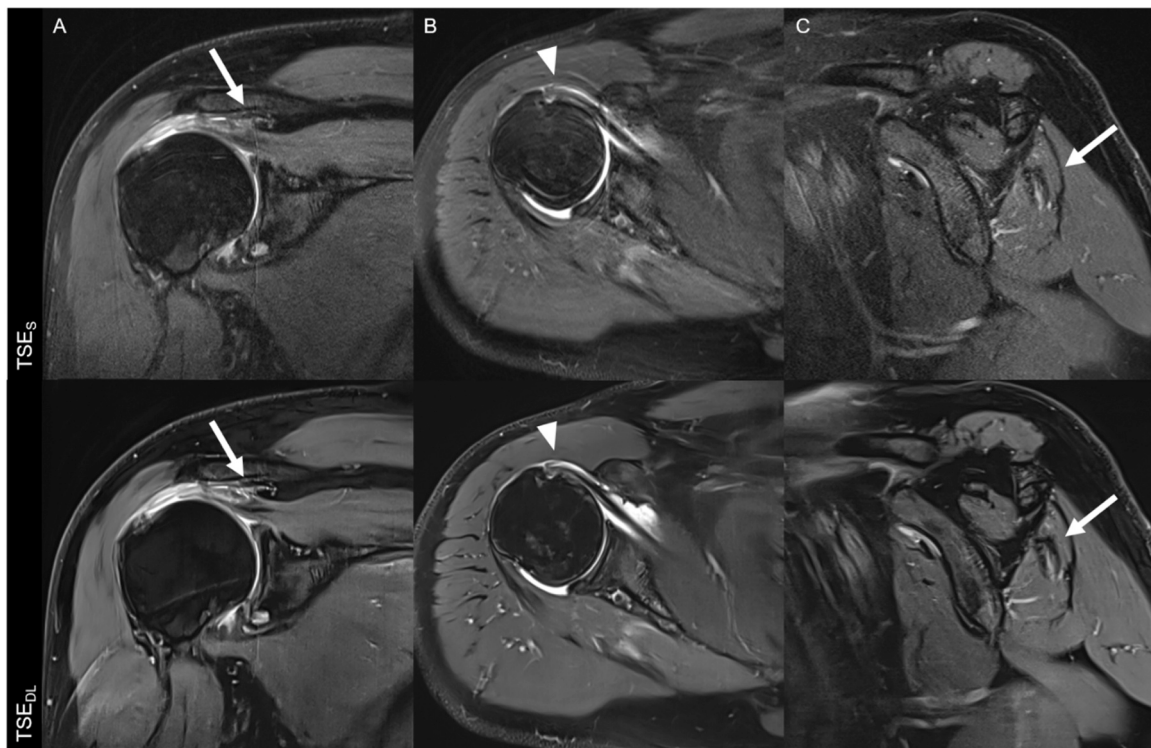


Fig. 4. Example of a standard (TSE_s, upper row) and accelerated, deep learning reconstructed (TSE_{DL}, lower row) shoulder MRI of the right shoulder at 3 Tesla of a 76-year-old patient with omalgia on the right side and suspected rotator cuff lesion at 3 Tesla. In the coronal PD-weighted TSE (A) you find a complete transmurular rupture of the supraspinatus tendon (arrow) which is well delineated in both sequences, but slightly sharper in the TSE_{DL}. In the axial PD-weighted TSE (B) the attachment tendinopathy of the subscapularis tendon (arrow head) is better delineated in the TSE_{DL} due to fewer motion artifacts, which in turn is attributed to the shorter acquisition time. The rupture of the infraspinatus muscle with tendon retraction in the PD-weighted TSE in sagittal oblique orientation (C) can be very well delineated in both sequences, with the TSE_{DL} providing improved sharpness and less noise.

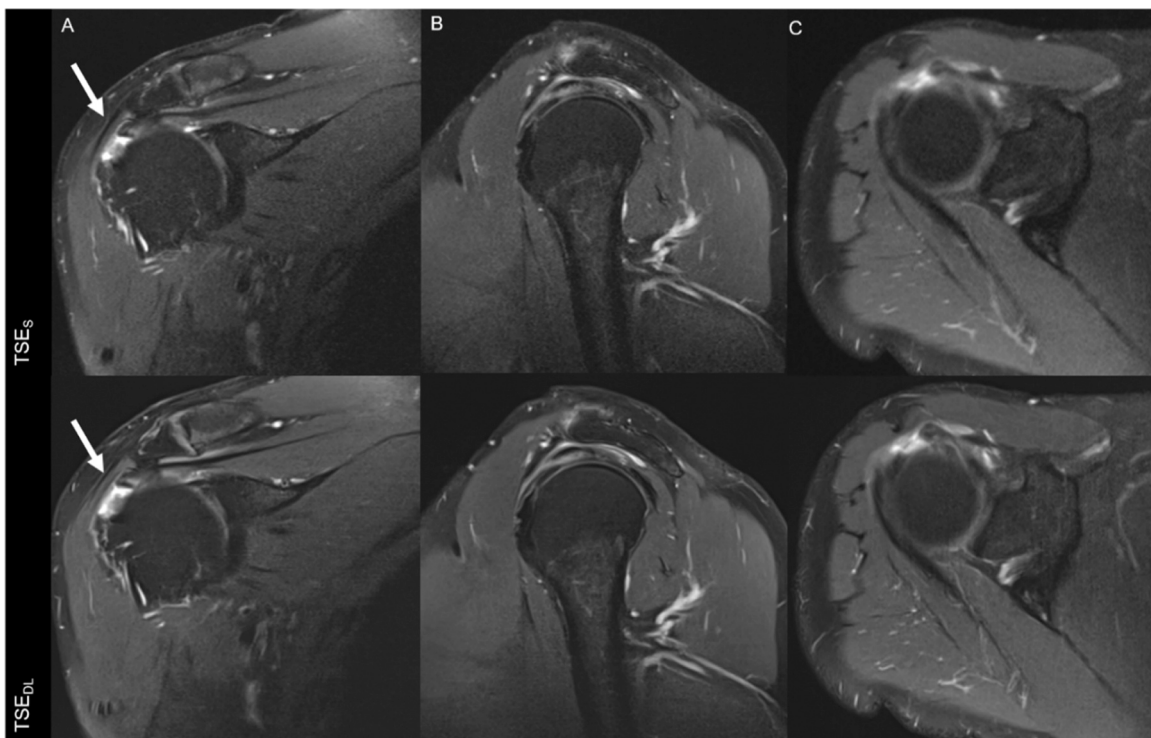


Fig. 5. Example of a standard (TSE_s, upper row) and accelerated, deep learning reconstructed (TSE_{DL}, lower row) shoulder MRI examination of a 58-year-old patient with shoulder pain and suspected rotator cuff rupture at 1.5 Tesla with PD-weighted TSE sequences in coronal (A), sagittal oblique (B), and axial (C) orientation. Rupture of the supraspinatus tendon with slight retraction (arrow) is seen, which is well delineated in both sequences, but slightly sharper in the TSE_{DL}. Noise is reduced in TSE_{DL} compared to TSE_s.

sequences were preferred for implementation. Third, although no significant difference in image impression was found between TSE_{DL} and TSE_S, readers were likely able to identify whether they were interpreting TSE_{DL} or TSE_S because of the characteristic appearance of the DL-reconstructed images. However, recall bias was minimized by randomization of datasets and a washout period of 30 days, before readers evaluated the second set of images of each patient.

In conclusion, a novel 5-minute TSE_{DL} protocol for the shoulder is feasible in daily clinical routine at 1.5 and 3 T and allows for a reduction in acquisition time of more than 50%, while improving image quality and maintaining equivalent diagnostic performance of shoulder abnormalities compared to standard TSE imaging. Therefore, TSE_{DL} may pave the way for the introduction of ultrafast protocols in shoulder MRI.

Funding

This research received no external funding.

Ethical statement

This prospective study was approved by the institutional review board (University of Tuebingen, clinical trial registry number: DRKS00023278) and written informed consent was obtained from all participants. All study procedures were in accordance with the Declaration of Helsinki and its subsequent amendments.

CRediT authorship contribution statement

You-Shan Feng: Writing – review & editing, Validation, Methodology, Investigation. **Judith Herrmann:** Writing – original draft, Visualization, Validation, Resources, Project administration, Methodology, Investigation, Formal analysis, Data curation, Conceptualization. **Andreas Lingg:** Writing – review & editing, Supervision, Methodology, Data curation, Conceptualization. **Gregor Koerzdoerfer:** Writing – review & editing, Software. **Jan-Peter Grunz:** Writing – review & editing, Validation, Supervision. **Sebastian Gassenmaier:** Writing – review & editing, Validation, Supervision, Project administration, Methodology, Investigation, Formal analysis, Data curation, Conceptualization. **Saif Afat:** Writing – review & editing, Visualization, Validation, Supervision, Resources, Project administration, Methodology, Investigation, Formal analysis, Data curation, Conceptualization. **Ahmed E. Othman:** Writing – review & editing, Validation, Supervision, Project administration, Formal analysis, Data curation, Conceptualization. **Dominik Nickel:** Writing – review & editing, Software. **Haidara Al-Mansour:** Writing – review & editing, Investigation, Formal analysis, Data curation.

Declaration of Competing Interest

The authors declare the following financial interests/personal relationships which may be considered as potential competing interests. Gregor Koerzdoerfer and Dominik Nickel are employees of Siemens Healthineers, Germany and provided the prototype Deep Learning reconstruction used in this study. Full control of patient data was with the authors of University of Tuebingen and who are not employees of Siemens

References

- I.P. Pappou, C.C. Schmidt, C.D. Jarrett, B.M. Steen, M.A. Frankle, AAOS appropriate use criteria: optimizing the management of full-thickness rotator cuff tears, *J. Am. Acad. Orthop. Surg.* 21 (12) (2013) 772–775.
- M. Lenza, R. Buchbinder, Y. Takwoingi, R.V. Johnston, N.C. Hanchard, F. Faloppa, Magnetic resonance imaging, magnetic resonance arthrography and ultrasonography for assessing rotator cuff tears in people with shoulder pain for whom surgery is being considered, *Cochrane Database Syst. Rev.* (9) (2013) CD009020.
- S.P. Daniels, S. Gyftopoulos, 3D MRI of the Shoulder, *Semin. Musculoskelet. Radiol.* 25 (3) (2021) 480–487.
- B. Hou, Y. Li, Y. Xiong, J.N. Morelli, J. Wang, C. Liu, G. Wu, X. Li, Comparison of CAIPIRINHA-accelerated 3D fat-saturated-SPACE MRI with 2D MRI sequences for the assessment of shoulder pathology, *Eur. Radiol.* 32 (1) (2022) 593–601.
- J.K. Kloth, M. Winterstein, M. Akbar, E. Meyer, D. Paul, H.U. Kauczor, M.A. Weber, Comparison of 3D turbo spin-echo SPACE sequences with conventional 2D MRI sequences to assess the shoulder joint, *Eur. J. Radiol.* 83 (10) (2014) 1843–1849.
- S.H. Lee, Y.H. Lee, H.T. Song, J.S. Suh, Rapid acquisition of magnetic resonance imaging of the shoulder using three-dimensional fast spin echo sequence with compressed sensing, *Magn. Reson Imaging* 42 (2017) 152–157.
- N. Subhas, A. Benedick, N.A. Obuchowski, J.M. Polster, L.S. Beltran, J. Schils, G. A. Ciavarrá, S. Gyftopoulos, Comparison of a fast 5-minute shoulder MRI protocol with a standard shoulder MRI protocol: a multi-institutional multireader study, *AJR Am. J. Roentgenol.* 208 (4) (2017) W146–W154.
- J. Herrmann, G. Koerzdoerfer, D. Nickel, M. Mostapha, M. Nadar, S. Gassenmaier, T. Kuestner, A.E. Othman, Feasibility and Implementation of a deep learning MR reconstruction for TSE sequences in musculoskeletal imaging, *Diagnostics* 11 (8) (2021).
- M.P. Recht, J. Zbontar, D.K. Sodickson, F. Knoll, N. Yakubova, A. Sriram, T. Murrell, A. Defazio, M. Rabbat, L. Rybak, M. Kline, G. Ciavarrá, E.F. Alaia, M. Samim, W.R. Walter, D. Lin, Y.W. Lui, M. Muckley, Z. Huang, P. Johnson, R. Stern, C.L. Zitnick, Using deep learning to accelerate knee MRI at 3T: results of an interchangeability study, *AJR Am. J. Roentgenol.* (2020).
- S. Hahn, J. Yi, H.J. Lee, Y. Lee, Y.J. Lim, J.Y. Bang, H. Kim, J. Lee, Image Quality and diagnostic performance of accelerated shoulder MRI with deep learning-based reconstruction, *AJR Am. J. Roentgenol.* 218 (3) (2022) 506–516.
- J. Herrmann, G. Keller, S. Gassenmaier, D. Nickel, G. Koerzdoerfer, M. Mostapha, H. Almansour, S. Afat, A.E. Othman, Feasibility of an accelerated 2D-multi-contrast knee MRI protocol using deep-learning image reconstruction: a prospective intraindividual comparison with a standard MRI protocol, *Eur. Radiol.* (2022).
- Y. Obama, Y. Ohno, K. Yamamoto, M. Ikeda, M. Yui, S. Hanamatsu, T. Ueda, H. Ikeda, K. Murayama, H. Toyama, MR imaging for shoulder diseases: Effect of compressed sensing and deep learning reconstruction on examination time and imaging quality compared with that of parallel imaging, *Magn. Reson Imaging* 94 (2022) 56–63.
- H. Almansour, J. Herrmann, S. Gassenmaier, S. Afat, J. Jacoby, G. Koerzdoerfer, D. Nickel, M. Mostapha, M. Nadar, A.E. Othman, Deep learning reconstruction for accelerated spine MRI: prospective analysis of interchangeability, *Radiology* (2022) 212922.
- K.M. Koch, M. Sherafati, V.E. Arpinar, S. Bhave, R. Ausman, A.S. Nencka, R. M. Lebel, G. McKinnon, S.S. Kaushik, D. Vierck, M.R. Stetz, S. Fernando, R. Mannem, Analysis and evaluation of a deep learning reconstruction approach with denoising for orthopedic MRI, *Radiol. Artif. Intell.* 3 (6) (2021) e200278.
- S. Gassenmaier, S. Afat, D. Nickel, M. Mostapha, J. Herrmann, A.E. Othman, Deep learning-accelerated T2-weighted imaging of the prostate: reduction of acquisition time and improvement of image quality, *Eur. J. Radiol.* 137 (2021) 109600.
- S. Gassenmaier, S. Afat, M.D. Nickel, M. Mostapha, J. Herrmann, H. Almansour, K. Nikolaou, A.E. Othman, Accelerated T2-weighted TSE imaging of the prostate using deep learning image reconstruction: a prospective comparison with standard T2-weighted TSE imaging, *Cancers* 13 (14) (2021).
- S. Gassenmaier, S. Afat, D. Nickel, M. Mostapha, J. Herrmann, A.E. Othman, Deep learning-accelerated T2-weighted imaging of the prostate: reduction of acquisition time and improvement of image quality, *Eur. J. Radiol.* (2021) 109600.
- D. Wessling, J. Herrmann, S. Afat, D. Nickel, A.E. Othman, H. Almansour, S. Gassenmaier, Reduction in acquisition time and improvement in image quality in T2-weighted MR imaging of musculoskeletal tumors of the extremities using a novel deep learning-based reconstruction technique in a turbo spin echo (TSE) sequence, *Tomography* 8 (4) (2022) 1759–1769.
- K. Hammernik, T. Klatzer, E. Kobler, M.P. Recht, D.K. Sodickson, T. Pock, F. Knoll, Learning a variational network for reconstruction of accelerated MRI data, *Magn. Reson. Med.* 79 (6) (2018) 3055–3071.
- F. Knoll, K. Hammernik, E. Kobler, T. Pock, M.P. Recht, D.K. Sodickson, Assessment of the generalization of learned image reconstruction and the potential for transfer learning, *Magn. Reson. Med.* 81 (1) (2019) 116–128.
- J. Schlemper, J. Caballero, J.V. Hajnal, A.N. Price, D. Rueckert, A deep cascade of convolutional neural networks for dynamic MR image reconstruction, *IEEE Trans. Med. Imaging* 37 (2) (2018) 491–503.
- M.L. McHugh, Interrater reliability: the kappa statistic, *Biochem. Med.* 22 (3) (2012) 276–282.
- N.A. Obuchowski, N. Subhas, P. Schoenhagen, Testing for interchangeability of imaging tests, *Acad. Radiol.* 21 (11) (2014) 1483–1489.
- E.F. Alaia, A. Benedick, N.A. Obuchowski, J.M. Polster, L.S. Beltran, J. Schils, E. Garwood, C.J. Burke, L.J. Chang, S. Gyftopoulos, N. Subhas, Comparison of a fast 5-min knee MRI protocol with a standard knee MRI protocol: a multi-institutional multi-reader study, *Skelet. Radiol.* 47 (1) (2018) 107–116.
- F. Zanchi, R. Richard, M. Hussami, A. Monier, J.F. Knebel, P. Omoumi, MRI of non-specific low back pain and/or lumbar radiculopathy: do we need T1 when using a sagittal T2-weighted Dixon sequence? *Eur. Radiol.* 30 (5) (2020) 2583–2593.
- L. Feng, T. Benkert, K.T. Block, D.K. Sodickson, R. Otazo, H. Chandarana, Compressed sensing for body MRI, *J. Magn. Reson Imaging* 45 (4) (2017) 966–987.

- [27] A. Defazio, T. Murrell, M.P. Recht, MRI Banding Removal via Adversarial Training, arXiv preprint arXiv:2001.08699 (2020).
- [28] T.O. Smith, B.T. Drew, A.P. Toms, A meta-analysis of the diagnostic test accuracy of MRA and MRI for the detection of glenoid labral injury, Arch. Orthop. Trauma Surg. 132 (7) (2012) 905–919.
- [29] L.L. Seeger, R.H. Gold, L.W. Bassett, H. Ellman, Shoulder impingement syndrome: MR findings in 53 shoulders, AJR Am. J. Roentgenol. 150 (2) (1988) 343–347.